Regional Geology of the Hypanis Valles System, Mars

Jacob Adler[1], James F Bell[2], Nicholas Hale Warner[3], Eldar Zeev Noe Dobrea[4], and Tanya N Harrison[5]

[1]Georgia Tech
[2]Arizona State University
[3]SUNY Geneseo
[4]Planetary Science Institute
[5]Planet Federal

November 22, 2022

Abstract

We present a geomorphic map of the Hypanis Valles watershed and a geomorphic map of the Hypanis deposit region at its terminus. We mapped these two regions at different scales: 1:2,000,000 for the catchment map (-5-10° N, 300-315° E) and 1:500,000 for the Hypanis deposit map (10-13.0° N, 313-316.5° E). Our mapping provides new morphologic insights beyond previous efforts which used lower spatial resolution data. We defined units based on morphology, albedo, thermal inertia, elevation, and spectral parameters. We propose that episodic volcanism and aqueous activity filled the Chryse basin from the early Noachian. Hypanis Valles was active during the Noachian, forming the Hypanis terminal deposits in the southern Chryse region. Hundreds of kilometer-sized mounds and cones stratigraphically post-date Hypanis fluvial deposition as these features appear to have erupted or effused through all other major map units. We propose sedimentary diapirism or mud volcanism may be responsible for these features, a hypothesis consistent with the compressional wrinkle ridge tectonism in a sedimentary basin. Future work could further investigate the formation of these cones and mounds and better assess their astrobiologic importance.

Regional Geology of the Hypanis Valles System, Mars

Jacob B. Adler[1], James F. Bell[2], Nicholas H. Warner[3], Eldar Noe Dobrea[4,5],

and Tanya N. Harrison[6]

[1]School of Earth and Atmospheric Sciences, Georgia Institute of Technology, Atlanta, GA 30332, USA.

[2]School of Earth and Space Exploration, Arizona State University, Tempe, AZ 85287, USA.

[3]Department of Geological Sciences, SUNY Geneseo, Geneseo, NY 14454, USA.

[4]NASA Ames Research Center, Moffett Field, CA 94035, USA.

[5]Planetary Science Institute, Tuscon, AZ, 85719, USA.

[6]Planet Federal, Washington, D.C., 20005, USA.

Key Points:

- We mapped the Hypanis Valles watershed and deposit region.
- Fan sediments were likely sourced from mid to late Noachian units with diverse lithologies.
- Cones and mounds suggest remobilization of buried sediments.

Corresponding author: Jacob Adler, `j.adler@gatech.edu`

Abstract

We present a geomorphic map of the Hypanis Valles watershed and a geomorphic map of the Hypanis deposit region at its terminus. We mapped these two regions at different scales: 1:2,000,000 for the catchment map (-5-10°N, 300-315°E) and 1:500,000 for the Hypanis deposit map (10-13.0°N, 313-316.5°E). Our mapping provides new morphologic insights beyond previous efforts which used lower spatial resolution data. We defined units based on morphology, albedo, thermal inertia, elevation, and spectral parameters. We propose that episodic volcanism and aqueous activity filled the Chryse basin from the early Noachian. Hypanis Valles was active during the Noachian, forming the Hypanis terminal deposits in the southern Chryse region. Hundreds of kilometer-sized mounds and cones stratigraphically post-date Hypanis fluvial deposition as these features appear to have erupted or effused through all other major map units. We propose sedimentary diapirism or mud volcanism may be responsible for these features, a hypothesis consistent with the compressional wrinkle ridge tectonism in a sedimentary basin. Future work could further investigate the formation of these cones and mounds and better assess their astrobiologic importance.

Plain Language Summary

We present a new geologic map of the largest proposed river delta deposit on Mars and the upstream region that contributed sediments. We investigate the source materials that Hypanis Valles eroded to better estimate the composition of units in the downstream deposits. We used high-resolution orbital images and datasets to map the region previously proposed as indication of an ocean shoreline 3.6 billion years ago. The terrain is more diverse than previous maps suggest, and some features may indicate recent eruption of buried sediments, providing additional targets for future study and exploration alongside the proposed delta.

1 Introduction

Orbital and landed spacecraft have observed widespread evidence of fluvial activity on early Mars including examples of former valley networks and paleolakes (Pieri, 1980; Carr, 1996; Goldspiel and Squyres, 1991; Cabrol and Grin, 1999, 2001; Howard et al., 2005; Irwin et al., 2005a, 2005b; Fassett and Head, 2005, 2008a, 2008b; Hynek et al., 2010). These processes were most active during the late Noachian/early Hesperian ($\sim 4.0 - 3.6$ Ga), after which time the climate of Mars rapidly shifted to more distinct episodes of fluvial activity

starting sometime between 3.8 – 3.4 Ga. (Fassett and Head, 2008a). The local details of this climate and geologic transition are varied and poorly understood. Many studies have argued that an ocean occupying the northern lowlands disappeared during this transition (Baker et al., 1991; Clifford & Parker, 2001), but the topic remains an open debate today.

Some examples of work in the last two decades that may support the northern ocean hypothesis include analysis of mineralogy, delta elevation, local geomorphology, and tsunami deposits (Di Achille & Hynek, 2010; Oehler & Allen, 2012; Rodriguez et al., 2016; Luo et al., 2017; Citron et al., 2018). Studies of the isotopic ratio of deuterium to hydrogen (D/H) indicates an ocean-sized volume of water has either escaped into space (Villanueva et al., 2015) or was buried in the crust (Scheller et al., 2021). On the other hand, no convincing examples of ancient shorelines have been identified to date despite advances in image resolution and orbital instruments (Sholes et al., 2019, 2021). While it is possible that global shoreline elevations have been warped over time (Perron et al., 2007; Citron et al., 2018), examination of the best examples of proposed "contact" elevations locally are still not consistent with shorelines (Sholes et al., 2021).

One intriguing feature that could potentially pin the shoreline location to the -2540 m elevation along the Chryse basin at 3.6 Ga is the Hypanis deposit (Fawdon et al., 2018; Adler et al., 2019). The significance of this deposit is that it is the largest proposed Martian delta to date, and has no northern topographic boundary. Thus, if Hypanis formed subaqueously then the northern lowlands of Mars must have been underwater. It is partly for these reasons that Hypanis was one of the landing site candidates for both the Mars 2020 and ExoMars rover missions.

Adler et al. (2019) and Fawdon et al. (2018) reported that the Hypanis deposit system is consistent with an ancient delta deposit based on geomorphic evidence, and that the progradation of deposits was due to shoreline retreat in Chryse Planitia. Distal deposits were found up to 130 km from the apex of the main lobe, and recorded a drop in water level of roughly 500 m. These initial studies identified mounds, mesas, and other unique units in the deposit region, but did not fully investigate the regional geology beyond the fan-deposit system. Furthermore, studies of the underlying composition and mineralogy of the main deposit were made difficult by extensive dust cover as well as dunes and/or transverse aeolian ridges (TARs). This work addresses 1) the composition of the fan-deposits by mapping the catchment materials that likely travelled through the Hypanis system, and 2)

the uncertainties in the timing and local geologic context of the deposits by mapping the basin floor material, dark flows, mesas, mounds, and other units surrounding the Hypanis deposits.

2 Background

2.1 Hypanis Deposit Geologic Context

The Chryse escarpment is the modified and potentially warped rim (see Citron et al., 2018) of the Chryse basin, which separates the Noachian highlands from Hesperian lowlands in the region. The Chryse basin currently has no topographic boundary in the north, and blends into the larger northern lowlands basin of Vastitas Borealis, although evidence exists defining the extent of the ancient impact structure (Pan et al., 2019).

Two regions of the Chryse basin have been explored by rover and lander spacecraft. The Viking I lander and Pathfinder lander with Sojourner rover have each explored the basin fill and superficial deposits above the Chryse basin. Buried ice and surface ice to the north of the Chryse region were observed by the Phoenix landed missions and from orbital studies (Arvidson et al., 2009; Smith et al., 2009). Slurry crater ejecta implying icy regolith is prevalent in this region, and as far south as the Noachian highlands in our mapped catchment region (Reiss et al., 2006).

The Chryse basin is filled with sedimentary and volcanic units. The sources of basin fill likely originate from valley network activity (4.0 - 3.2 Ga), a proposed series of northern oceans (see Parker, 1994; Carr, 1996; Head et al., 1998; Clifford and Parker, 1999; Carr, 2000; Carr and Head, 2009, and references therein), Hesperian volcanism (3.6 Ga), outflow channels (3.2 Ga), and other events. Previous geologic and geomorphic maps of the region are at a much larger scale than those produced in this work and are based on various imaging datasets at lower spatial resolution (see Scott and Carr, 1978; Scott and Tanaka, 1986; Rotto and Tanaka, 1995; Tanaka et al., 2014.)

2.2 Previous Work on the Hypanis Deposit

The first work providing a detailed analysis of the Hypanis deposit was Hauber et al. (2009). The authors found it difficult to determine whether the Hypanis and Sabrina deposits were alluvial or deltaic based on a lack of clear evidence for a standing water level such as terraces, shorelines, or a delta front (Hauber et al, 2009). They also interpret
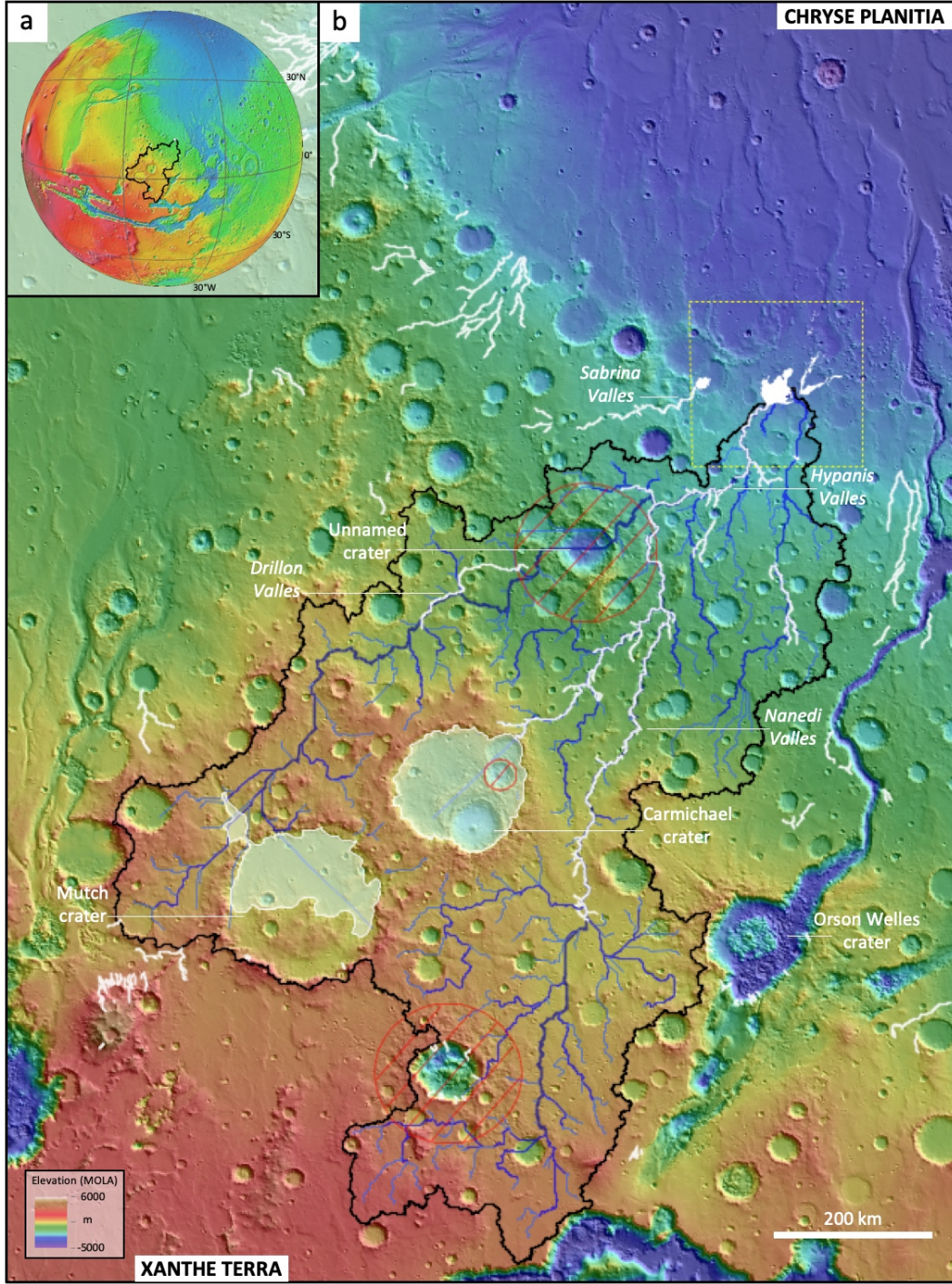
Figure 1: Hypanis deposit, Mars. North is up in all images. (a) The catchment area for this study (black outline) is larger than for most Martian deltas, stretching from Valles Marineris to the Chryse escarpment. (b) Elevation map of the Hypanis catchment reproduced from Fawdon et al., 2018 using ArcMap hydrology tools on a HRSC/MOLA blended DEM. The Hypanis and Sabrina deposits are shown in white as are valley networks that were previously mapped. Extrapolated stream orders are shown in shades of blue and are roughly consistent with CTX image analysis. Paleolakes (transparent white) were likely present in large craters based on outlet features. Craters postdating valley networks and thus excluded from paleocatchment composition analysis are marked in red. The location of the deposit map region is marked in yellow.
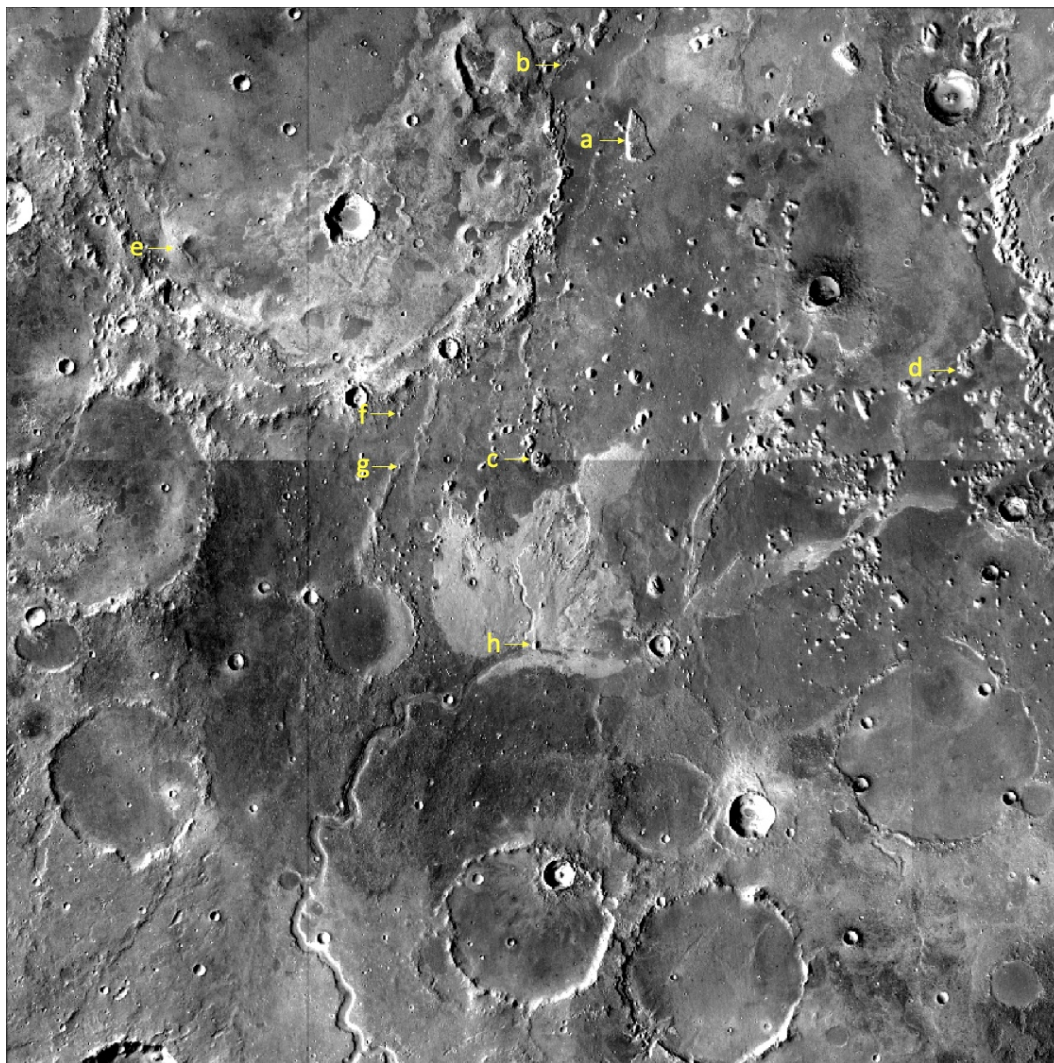
Figure 2: CTX global mosaic basemap utilized for mapping the Hypanis deposit, Mars. Unit example locations from Figure 5 are marked in yellow. Image is 200 km across.

that the Hypanis deposit was fed by the combination of both Hypanis Valles and Nanedi Valles, which were connected at that time, thus explaining the large volume of the Hypanis deposits. Subsequently, Kleinhans et al. (2010) presented a model for forming the neighboring Sabrina deposit as an alluvial fan, with a short timescale of formation. Later, Adler et al. (2019) and Fawdon et al. (2018) have provided measurements in support of the deltaic formation hypothesis for Hypanis, and argue that Sabrina was likely similarly formed. These works found a progressive basinward advance of the channel-lobe transition, plausible avulsion node migration, and stacks of roughly horizontal sediment layers indicating a subaqueous environment. These studies noted a lack of evidence of the characteristic alluvial fan architecture, but also did not identify a clear topset-foreset slope transition, a common diagnostic tool for deltas. It could be because of the unprecedented size of the deposit and high rates of subsequent erosion that this transition would not be preserved (Adler et al., 2019).

The timing of the Hypanis deposition was dated both from Context Camera (CTX)-derived impact crater statistics in the catchment on an ejecta blanket that superposes Hypanis Valles, and from buffered crater counts on Hypanis Valles. Both methods were consistent with previous age constraints and place the Hypanis deposit as older than 3.6 Ga (Fawdon et al., 2018). The presence of surrounding units including dark flows, wrinkle ridged plains, mesas and mounds, were noted but their stratigraphy and timing relative to Hypanis were not examined in detail. Adler et al., 2019 posited that the plethora of rounded buttes observed mostly in the northern portion of the study region could potentially represent former crater rim remnants, thus allowing for a land dam to enclose Hypanis in a local basin. This current work reassesses that possibility as detailed mapping has led to an improved interpretation of surrounding units.

In this work we mapped the surroundings of the Hypanis deposit and the units that Hypanis and Nanedi Valles carved through. As a result, we have created a comprehensive list of the materials potentially present in the deposit, and present a better understanding of the regional geologic history surrounding the largest potential delta on Mars.

3 Data and Methods

3.1 Geomorphic Mapping

We divided mapping into two regions, a deposit region and a catchment region. The deposit region maps serve to characterize the geology and geomorphology of the units immediately surrounding the Hypanis fan-shaped layered deposit. Two maps of the deposit region were produced: a major unit map to display the floor units and large scale trends (Figure 3) and a detailed map including features as small as ∼ 500 m in size (Figure 4). The deposit maps cover the area from 10-13.5°N, 313-316.5°E, and are 1:500,000 in scale. We used a CTX global mosaic (6 m/pix) as a basemap for drawing contacts and shapes (Dickson et al., 2018). The global CTX map was streamed in JMARS (Java Mission-planning and Analysis for Remote Sensing; Christensen et al., 2009), and individual 4°x4° CTX mosaic tiles were also uploaded to JMARS for enhanced control of color stretching. Units were defined based on a variety of strict quantitative and qualitative guidelines from other datasets which were processed, projected, overlayed, and aligned to the basemap (e.g. albedo, thermal inertia, spectral parameters, and morphology) described further in the description of map units (Tables 1-3).

A map of the catchment region was also produced, containing features down to a size of 5 km in a similar quantitative and qualitative fashion. The 5 km size limit was chosen because of the large area of the catchment. The catchment map contains the major units that comprise the floor materials that may have travelled down Hypanis Valles and into the Hypanis deposit and deposit region. Several units are discussed within the context of the Tanaka et al. (2014) global geologic map of Mars. For consistency with similar work, some unit names and morphologies follow the same mapping conventions presented in Goudge et al. (2015) of Jezero crater and its watershed. All unit mapping was performed in JMARS v.4.0.20.

To define the paleo-catchment boundary (Figure 1), we used ArcMap (esri, 2011) Hydrology tools in a similar fashion to Fawdon et al. (2018). We utilized the High Resolution Stereo Camera (HRSC) and Mars Orbiter Laser Altimeter (MOLA) Blended Global Digital Elevation Model (DEM) v2 created by the USGS for the initial catchment surface, whereas the prior model was based on the MOLA Global DEM at a lower resolution. Sinks in the DEM were filled before a pour point was selected and streams calculated. The pour point was chosen on the eastern side of Hypanis to include channels relevant to the main lobe and

braided channels. Both the Hypanis and Nanedi systems were likely connected at the time of formation of the Hypanis deposit, and this was included in the model. The watershed was thus defined as the area that topographically drains into the pour point. Areas in the catchment that postdate Hypanis Valles are marked in Figure 1. Despite the increased resolution of the catchment DEM, the resulting stream network is roughly identical to the one previously presented in Fawdon et al., 2018.

In the deposit map region, higher resolution DEMs were available. We utilized multiple products from High Resolution Imaging Science Experiment (HiRISE) and CTX stereopairs that were previously described in Adler et al. (2019) including our derived regional DEM mosaic for perspective views of units, height and volume measurements, and stratigraphic contact investigations.

Several units are defined by their Thermal Emission Imaging System (THEMIS) TI (thermal inertia) and nighttime temperature. The THEMIS Global Day, Night, Night/Day, and TI mosaics were often used to assist with locating unit contacts, and were useful for capturing the extent of impact crater ejecta. Higher resolution THEMIS Day, Night, and Night/Day mosaics were utilized in the deposit map region (USGS, R. Fergason 2006).

The interpreted cross section (Figure 10) includes the topographic profile derived from our DEM mosaic of the deposit region in JMARS. For clarity visualizing the stratigraphic sequence, the original high resolution noisy profile was smoothed in areas using the simplify function in Inkscape and deleting outlier values.

3.2 Mineralogic Mapping

Previous study of the mineralogy of the Hypanis deposit was limited due to the widespread cover of dust, dunes, and TARs. Furthermore, high resolution targeted CRISM (Compact Reconnaissance Imaging Spectrometer for Mars) observations are limited to only a few locations in the region. To further assess the potential compositions over such a large region of Mars, we utilized lower resolution spectral products with near global coverage including TES (Thermal Emission Spectrometer) derived mineral maps (at 4 ppd equal to $\sim$ 14 km/pixel) and CRISM Multispectral Survey (MSP) images (200 m/pixel). Previous analysis of MSP and FRT (Full Resolution Targeted) observations in the deposit map region was also incorporated (Adler et al., 2019). In previous work, we found that the High-Calcium Pyroxene and the D2300 parameters were the most useful mapping indicators in the deposit

map region. The TES and CRISM-derived mineral identifications were divided into two categories: confirmed and unconfirmed (Figure 9).

Previously published mineral occurrences that had been analyzed locally in detail are marked as confirmed observations. Confirmed mineralogy included observations of hydrated silica, kaolinite, and feldspar [Wray et al., 2013; Carter and Poulet, 2013; Pan et al., 2021]; hydrated sulfate, phyllosilicate [Carter et al., 2015, Ehlmann and Edwards, 2014 and references therein]; and phyllosilicate (green in Figure 9) [Adler et al., 2019].

TES global mineral occurrences, although published and only displayed when above the detection threshold of 10%, are marked unconfirmed, as the individual pixels have not been thoroughly examined locally to our knowledge. Unconfirmed mineralogy included observations of phyllosilicate [CRISM MSP, D2300 parameter > 0.05]; hematite [TES Hematite Abundance > 0.10, Bandfield, 2002]; olivine [TES Olivine Abundance > 0.10, Koeppen and Hamilton, 2008]; high-Ca pyroxene [TES HCP Abundance > 0.10, Bandfield, 2002]; phyllosilicate/hi-Si glass [TES High-Si Glass Abundance > 0.10, Bandfield, 2002]; and plagioclase [TES Plagioclase Abundance > 0.10, Bandfield, 2002]. Where multiple TES mineral abundance maps were above the 0.10 detection threshold described in Bandfield, 2002 for a given pixel, the color was marked according to the legend.

4 Results

4.1 Chryse Basin Units - "Deposit Map"

Within the southern Chryse basin area covered by the deposit map (Figures 3-4), major units range from the mid-Noachian to early-Hesperian and possibly younger. The floor material to the south is generally older, and material to the north progressively younger. In the Tanaka et al. (2014) global geologic map of Mars the Hypanis deposit region spans three major units: mid Noachian highlands (mNh), late Noachian highlands (lNh), and early Hesperian transition (eHt). In our mapping, we reassessed the contacts between these units, and identified additional unit types.

In the global map, mNh and eHt are separated by only one unit, lNh. We distinguished four floor units (Cs, lNh, Lf1, and Lr) that spatially and temporally separate the bulk of Xanthe Terra from Chryse Planitia. Otherwise, mNh and eHt follow the same descriptions and interpretations as presented in Tanaka et al., 2014.

Figure 3: Geomorphic map of the major units in the Hypanis deposit region. The legend below shows which units are based on Tanaka et al., 2014 and which are new based on this work. See the description of map units table for more information. Background is a CTX mosaic (6 m/pixel).

To the north of mNh, the Chryse skirt unit (Cs) lies along the Chryse escarpment. This unit has a strong slope component and connects the highlands elevations to the lower plains. Cs is also marked by a high THEMIS nighttime temperature and high thermal inertia. In Adler et al., 2019, regionally mapping of CRISM MSP images showed Fe/Mg phyllosilicate signatures in the deposit region. From our mapping, most of these phyllosilicate bearing materials occur in the Cs unit. The teal color within the Cs and Lr units in Figure 4, shows the locations of the phyllosilicate-bearing material.
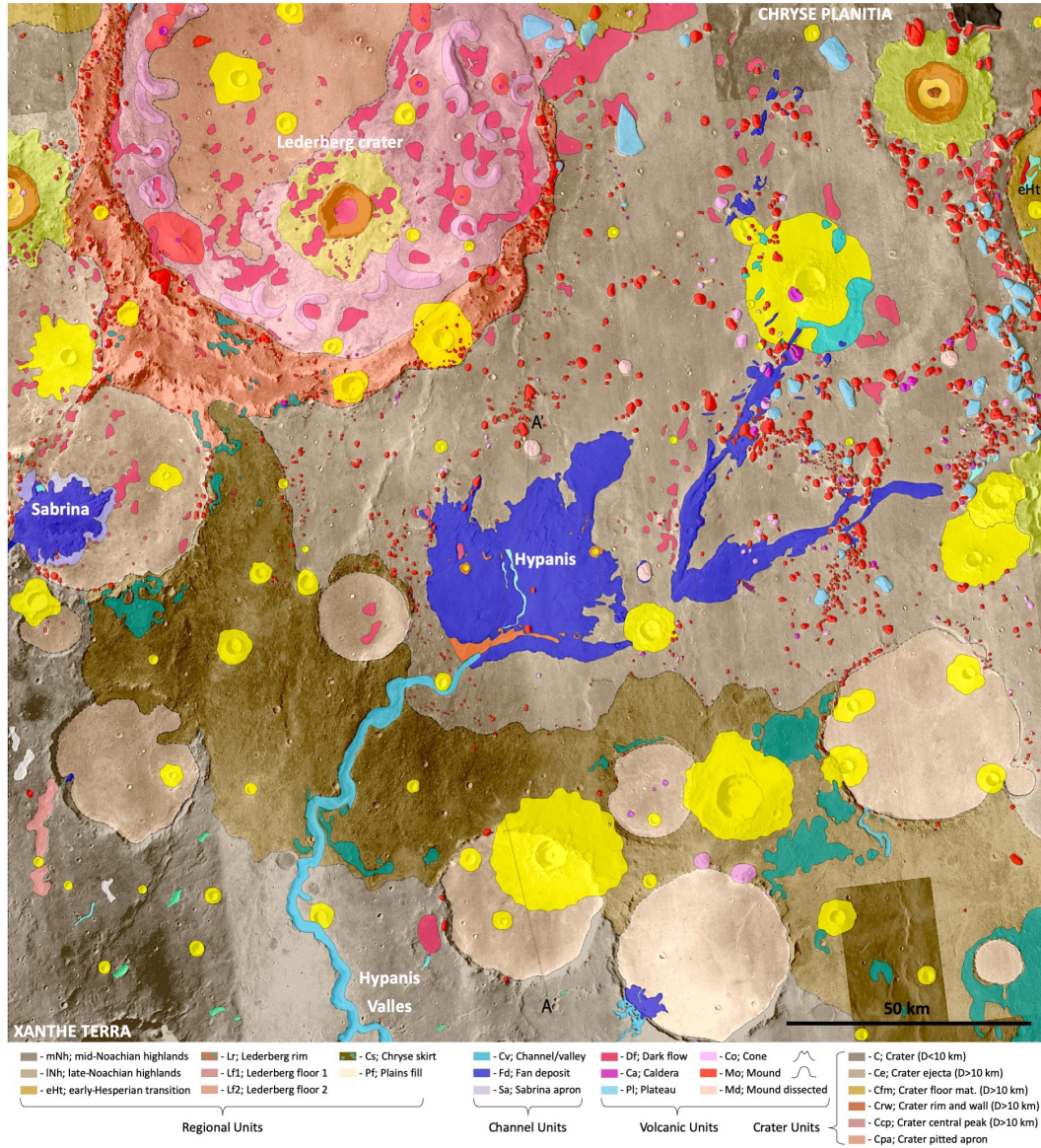
Figure 4: Geomorphic map of the Hypanis deposit region. The legend below shows units within this deposit map. See the description of map units table for more information. Background is a CTX mosaic (6 m/pixel).

Major Units Within the Hypanis Deposit Region

Unit Map Symbol	Unit Name	Unit Description	Unit Interpretation
mNh	mid-Noachian highlands	"Heavily cratered and marked by locally dense valleys, grabens, and wrinkle ridges" - Same as *Tanaka et al., 2014* [mNh]	"Undifferentiated impact, volcanic, fluvial, and basin materials. Moderately to heavily degraded" - Same as *Tanaka et al., 2014* [mNh]
Cs	Chryse skirt	High THEMIS thermal inertia sloping unit along the Chryse escarpment. Divides cratered highlands from lowlands. Phyllosilicate bearing.	Altered Chryse basin unit stratigraphically below lNh.
lNh	late-Noachian highlands	Mostly plains forming. Marked by grabens and wrinkle ridges. Includes cones, mounds, and mesas. May be tens to hundreds of meters thick. - Reassessment of *Tanaka et al., 2014* [lNh and eHt]	"Mass-wasting, fluvial/lacustrine, and other sedimentary materials and possibly volcanic rocks in places. Tectonically contracted." Containing large volcanic eruption features. - Reassessment of *Tanaka et al., 2014* [lNh and eHt].
eHt	early-Hesperian transition	"Plains-forming deposits, undulating to moderately rugged; includes scattered low knobs and mesas...moderate density of wrinkle ridges" - Same as *Tanaka et al., 2014* [eHt]	"Mass-wasting, fluvial/lacustrine, and other sedimentary materials and possibly volcanic rocks in places. Tectonically contracted." Stratigraphically between lNh and *Tanaka et al., 2014* [Hto]. Brighter than lNh and does not contain outflow signature of [Hto]. - Same as *Tanaka et al., 2014* [eHt].
Lr	Lederberg rim	High relief unit with light toned ridges, mounds, and darker valleys. Phyllosilicate bearing.	Combination of Lederberg rim materials, surrounding plains cover, and erupted mound material along former crater rim.
Lf1	Lederberg floor 1	Light toned floor with dark patches in topographic lows associated with quasi-circular cones or craters.	Eruptions and associated flows as described by *Brož and Hauber, 2013*.
Lf2	Lederberg floor 2	Lightly cratered smooth plains within Lederbeg crater	Plains material partially covering Lf1. Similar to flat regions within units eHt, Pf, and lNh.
Pf	Plains fill	Flat lying plains with few small craters and raised circular perimeter	Plains fill of degraded large Noachian impact craters.
Cd	Channel deposits	Layered light toned fan-shaped unit at the terminus of valleys	Combination of fan units Fd and Sa.

Table 1: Description of major geomorphic map units in deposit region.

Cs is found elsewhere along the edge of the Chryse basin outside of the mapped deposit region, extending up to 400 km to the northwest along the Chryse escarpment. Outside of the mapped region to the northwest, Cs appears to be the only major unit dividing the Noachian highlands from the Hesperian plains.

The 90 km Lederberg crater in the deposit map region is heavily modified by surface deposits and volcanism. We mapped three units within this complex: the Lederberg rim (Lr) and two Lederberg floor units (Lf1, Lf2). Features in Lederberg crater are investigated in detail in Brož and Hauber, 2013. In our mapping, we distinguished Lr as having a high elevation, following the curved crater rim shape, having ridges with high relief, darker valleys, and a multitude of small mounds. Lf1 is lighter-toned than its surroundings and contains dark patches in topographic lows associated with quasi-circular crater/cone rims. Lf2 is a smooth plains unit that is lightly cratered.

Geomorphic Units Within Hypanis Deposit Region

Unit Map Symbol	Unit Name	Unit Description	Unit Interpretation
Crater Units			
C	Crater (D < 10 km)	Crater ejecta, rims, and floor material of all craters with a diameter 1-10 km.	Impact crater and associated deposits of diameter 1-10 km.
Ccp	Crater central peak (D > 10 km)	Blocky, uplifted central peak material within craters with a diameter > 10 km.	Central peaks of impact craters with a diameter > 10 km.
Cfm	Crater floor material (D > 10 km)	All material associated with floors of craters with a diameter > 10 km.	Floor material of impact craters with a diameter > 10 km.
Ce	Crater ejecta (D > 10 km)	Rough ejecta material that shows radial textures from the crater that emplaced it.	Ejecta of craters with a diameter > 10 km. Deposits may also have small patches of
Crw	Crater rim and wall (D > 10 km)	Blocky rim and wall material associated with craters with a diameter > 10 km.	Rim and wall materials of impact craters with a diameter > 10 km.
Cpa	Crater pitted apron	Eroded, pitted unit along (Ce) where presumably mantling fan deposits (Fd).	Eroded and pitted impact crater ejecta where presumably mantling fan deposits.
Channel Units			
Cv	Channel/valley	Valley networks consistent with the global database [*Hynek et al., 2010*] and smaller local valleys.	Fluvially carved river valley network consistent with the global database [*Hynek et al., 2010*].
Fd	Fan deposit	Layered, light-toned unit that composes Hypanis, Sabrina, and other smaller local fan-shaped deposits at the terminus of valleys (consistent with *Adler et al., 2019*; *Fawdon et al., 2018*).	Eroded deltaic deposit of fine sediment. Inverted braided channel fill. Distal fluvial deposits.
Sa	Sabrina apron	Polygonally fractured terrain along the border of the Sabrina fan-shaped deposit (consistent with *Knade et al., 2017*).	Eroding and partially exhumed fan deposit (Fd) and other crater fill.
Volcanic Units			
Df	Dark flow	Lower albedo, crater-retaining unit with flow-like margins. Present in topographic lows and as a capping unit.	Volcanic unit with low albedo present in small patches and regionally widespread.
Ca	Caldera	Conical feature with large central crater and low or collapsed rim.	Volcanic explosive eruption or collapse product.
Co	Cone	Conical mound (400 m - 2 km diameter) with a large or visible central crater.	Sedimentary or igneous volcanic cone with central crater.
Mo	Mound	Predominantly light-toned mound (400 m - 2 km diameter) with small pits.	Sedimentary or igneous volcanic mound with small pits.
Md	Mound dissected	Large mound with radial dissection, faulting, or collapse.	Large sedimentary or igneous volcanic mound.
Pl	Plateau	Mesa higher than most mounds and larger (diameter > 2 km) with irregular shapes (not round).	Large block of from higher standing sedimentary or volcanic unit that has been heavily eroded.

Table 2: Description of geomorphic map units in deposit region.

The plains fill unit (Pf) is similar to Lf2 but occurs outside of Lederberg crater and appears on top of mNh, Cs, and lNh. Pf is marked by flat lying plains with few small craters and sometimes a raised circular perimeter. The channel deposits (Cd) are light-toned, layered, low thermal inertia, fan-shaped units discussed in previous works. Finally, the late-Noachian highlands (lNh) unit is reassessed for this work and mixes some of the characteristics from each of the Tanaka et al., 2014 lNh and eHt units. We map lNh as a mostly plains forming unit containing grabens, wrinkle ridges, cones, mounds, and mesas.

Within the southern Chryse basin covered by the detailed deposit map (Figure 4), geomorphic units appear to belong to four categories: Channel, Volcanic, Crater, and Regional. The regional units were described above and are the major units mapped in Figure 3. Channel units (Cv, Fd, Sa) were mapped and described in detail in several other works

including Hauber et al., 2009, Fawdon et al., 2018 and Adler et al., 2019. The channel units
are colored in shades of blue and mark the sinuous channels and deposits at their termini.
Crater units (C, Ce, Cfm, Crw, Ccp, Cpa) are colored in shades of yellow and brown, and
are subdivided for craters larger than 10 km to follow the same naming convention and
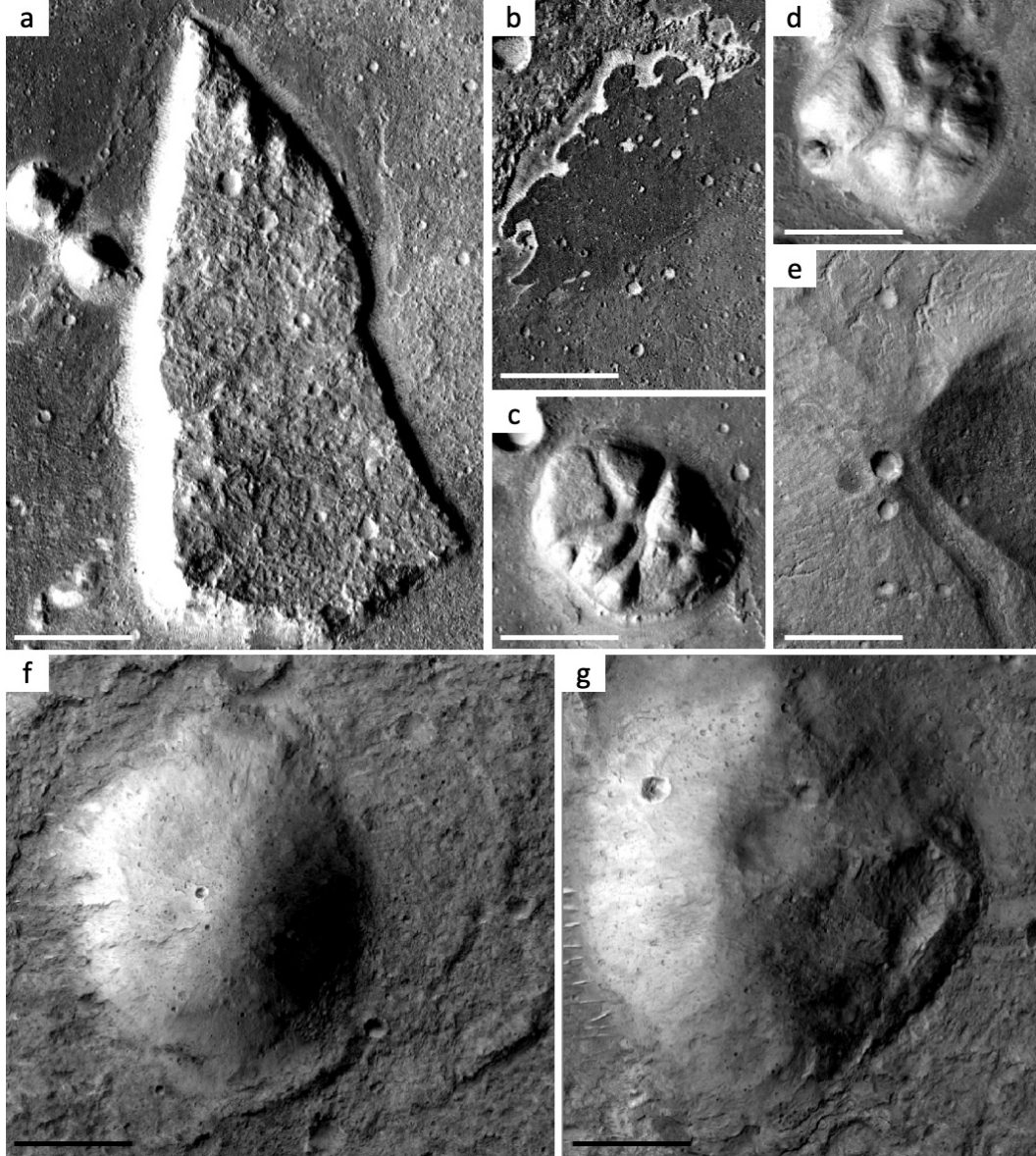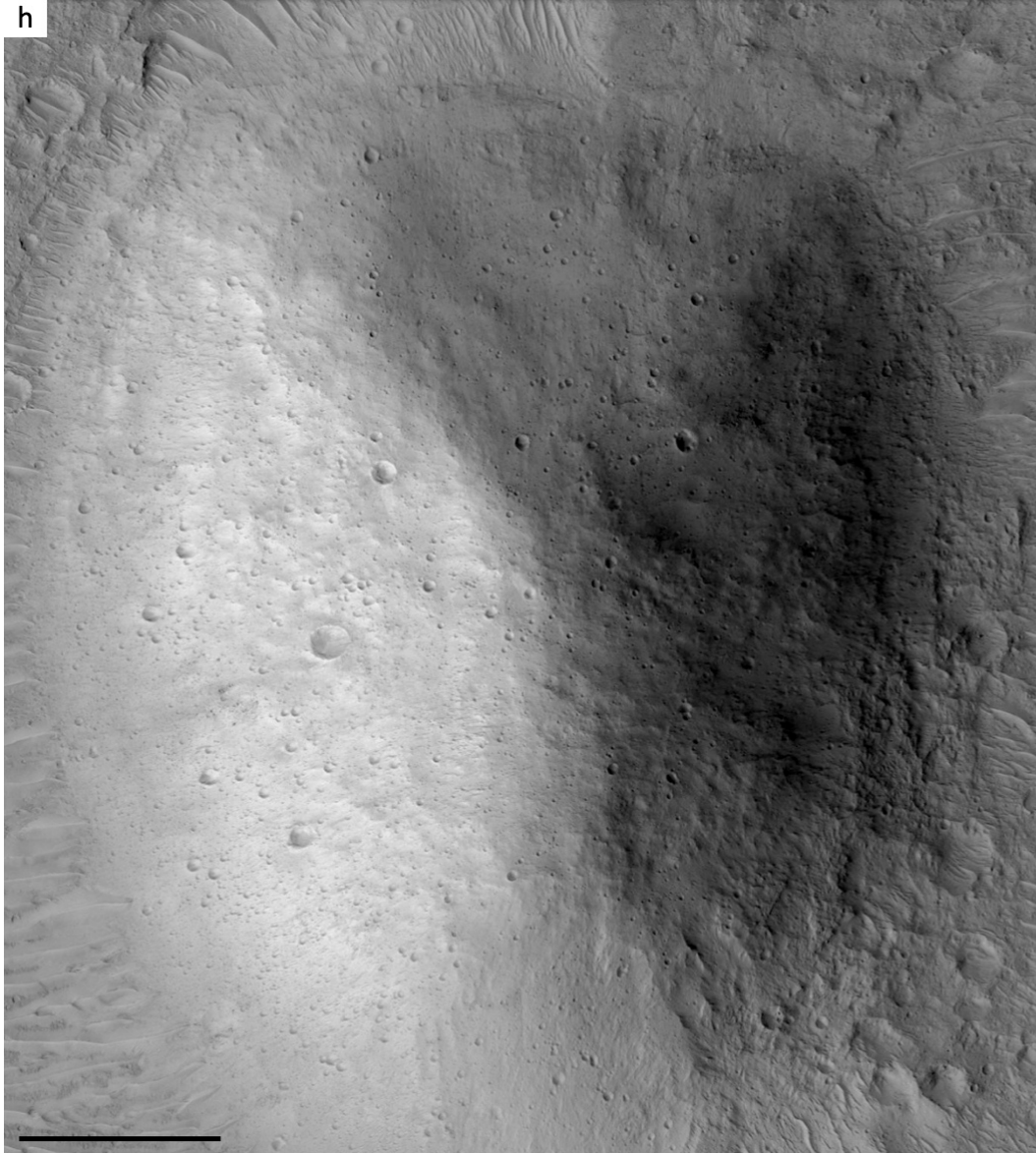description as crater units in Goudge et al. (2015).

Figure 5: Example volcanic units within the deposit map region. a) plateau, b) dark flow, c-d) dissected mounds, e) caldera atop volcanic edifice, f) mound, g) cone, h) mound. White scale bars are 2 km, black scale bars are 250 m. Example unit locations are marked in Figure 2, unit descriptions and interpretations are listed in Table 2.

₂₆₄ Here we describe in detail the Volcanic units (Df, Ca, Co, Mo, Md, Pl) mapped in

₂₆₅ Figure 4. The term volcanism is used in the general sense, as we consider a variety of

₂₆₆ formation mechanisms including mud volcanism, igneous volcanism, and volatile release.

₂₆₇ Examples of each of these units are shown in Figure 5. Dark flows (Df) have a low albedo

₂₆₈ and higher thermal inertia than their surroundings. Df is a crater-retaining unit often found

₂₆₉ as a capping unit or in topographic lows and with flow-like margins. Calderas (Ca) are cone

₂₇₀ shaped or oblong and have a large central crater with a low or collapsed rim. Most calderas

are within the Lederberg floor unit (Lf1) as summits of presumed volcanic edifices, or within the late-Noachian highlands (lNh) plains.

Cone (Co) and Mound (Mo) units are distinguished from each other by their topographic profile and CTX or HiRISE morphology. Cones and mounds range in diameter from roughly 400 m to 2 km, and have small pits on their surface in HiRISE images. Cones (Co) have clear summit craters in CTX or HiRISE images and/or a topographic profile indicating a central depression, while Mounds (Mo) do not have summit craters. However, where HiRISE coverage exists, many mounds appear to have a small central pit at their peak, as well as pits distributed across the surface. Dissected mounds (Md) are large mounds with a roughly radial dissection, faulting, or collapse. Plateaus (Pl) are mesas larger than 2 km with non-round shapes and usually taller than cones or mounds.
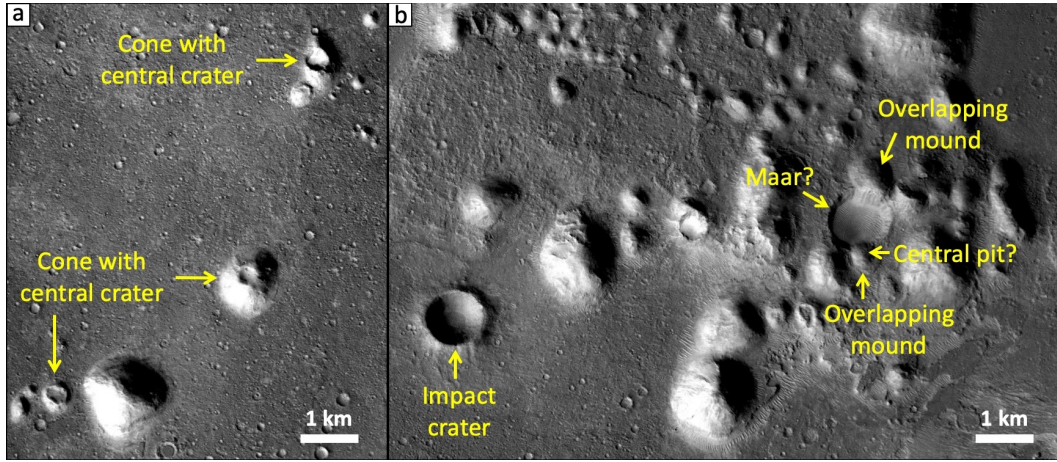

Figure 6: a) Cones of various sizes and degradation (unit Co). b) A field of cones, mounds, and potential maars are interpreted as the youngest units. They appear to have erupted through the major floor units mapped in Figure 3.

4.2 Hypanis Deposit Units - "Catchment Map"

Within the Hypanis watershed region in Xanthe Terra covered by the catchment map, major units span from the early Noachian to the Hesperian. Most of the catchment floor is composed of mid-Noachian highlands (mNh) and early-Noachian highlands (eNh), described Tanaka et al. (2014) and re-mapped for this work. Early-Noachian highlands occur as isolated regions that are more heavily cratered and with greater relief than mNh. Large craters with a diameter greater than 50 km are labeled as unit (C) where their ejecta and morphology are not majorly degraded or buried. One difference from previous maps is the

extent of ejecta from the "Unnamed crater" in Figure 1. Ejecta from this crater, designated as crater 15N in previous work, superposes the Hypanis Valles western branch, and thus postdates the formation of Hypanis Valles and the Hypanis deposit (Fawdon et al., 2018). The Smooth floor unit (Sf) is similar to the Tanaka et al., 2014 global map unit [eHh] and appears to embay the Rough intracrater unit (Ri). Other major floor units that are mapped only in the catchment include the Southern plains (Sp), Raised lineated (Rl), and Valles Marineris skirt (Vms) units. These three units cover a limited area and are located near the southern end of the catchment. Because these units do not appear to have once covered a farther extent to the north and are likely of a younger age than Hypanis Valles activity, their contribution to sediment transport down Hypanis Valles in the late Noachian is unlikely.

Within the mNh, eNh, and other major catchment units mapped and described above, several crater morphologies are observed. Craters with slurry ejecta and craters with ejecta and central pits are common throughout the catchment region. Craters with floor fill appear significantly buried or modified and are also ubiquitous in the catchment region. Craters with a chaos floor are found only in few locations and near the eastern border of the catchment. Craters with pedestal style ejecta blankets are much smaller in diameter than the previously mentioned catchment craters and are widespread. A few smaller diameter craters have either dark ejecta or a young appearance with rays.
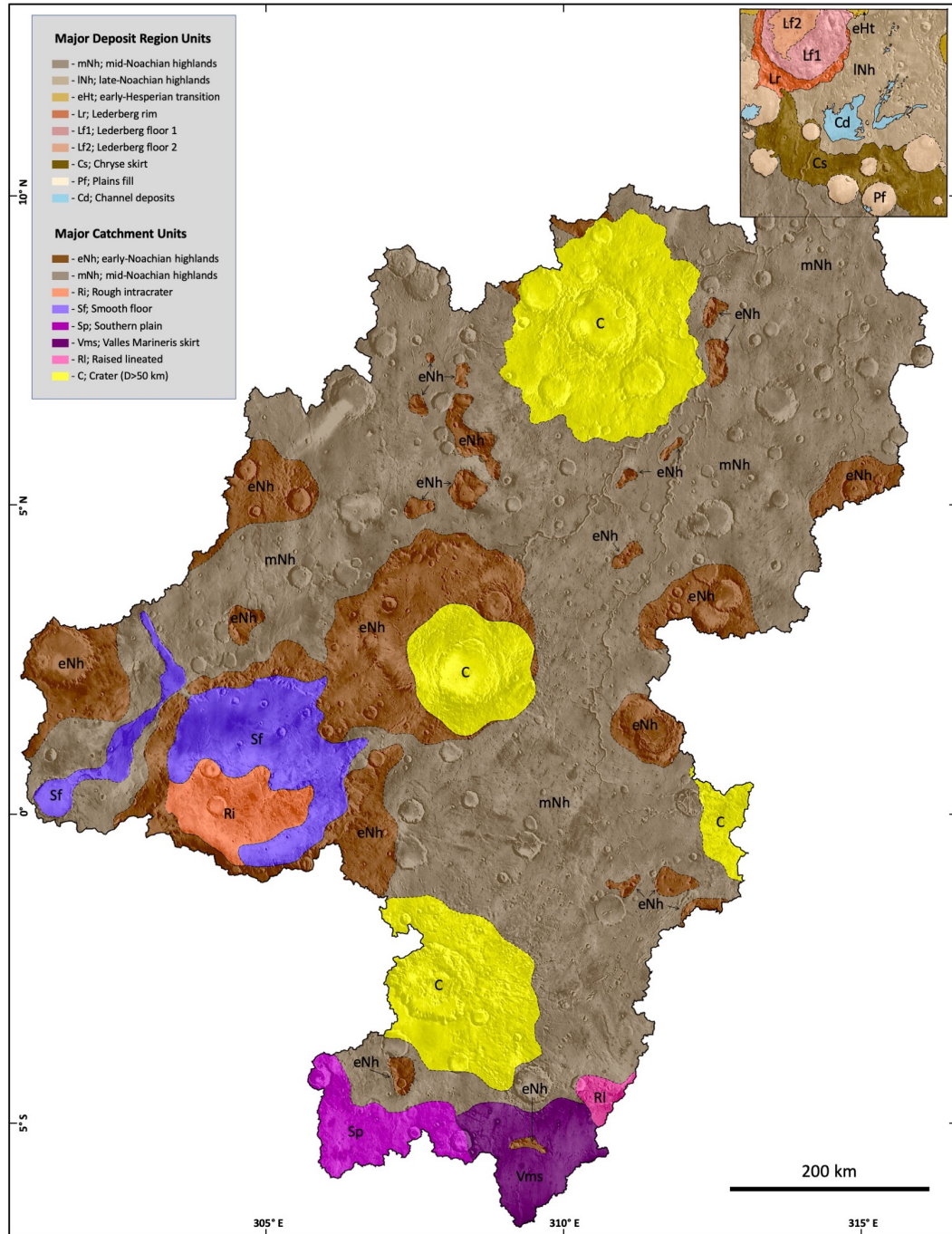
Figure 7: Geomorphic map of the major units in the Hypanis deposit catchment. See the description of map units table for more information. Background is THEMIS global daytime infrared mosaic (100 m/pixel).

Major Units Mapped Only Within the Hypanis Catchment Region

Unit Map Symbol	Unit Name	Unit Description	Unit Interpretation
eNh	early-Noachian highlands	Heavily cratered, often isolated regions of higher topography and relief. Same as *Tanaka et al., 2014* [eNh]	"Undifferentiated impact, volcanic, fluvial, and basin materials. Heavily degraded; tectonically deformed in places" - Same as *Tanaka et al., 2014* [eNh].
Ri	Rough intracrater	Rough cratered terrain within large degraded crater.	Similar to eNh with moderate to low THEMIS nighttime temperature.
Sp	Southern plains	Ridged patchy plains lightly to moderately cratered.	Similar to (Np) and (eNh), but more patchy morphology and no valley networks.
Rl	Raised lineated	Locally high elevation of wide linear ridge with filled and unfilled craters.	Ridge unit that extends to NE out of catchment.
C	Crater	Large crater with ejecta. D > 50 km.	Impact crater and associated deposits. Diameter > 50 km.
Sf	Smooth floor	"Plains-forming, relatively smooth outcrops...Occurs on plateaus surrounding Tharsis rise and in scattered highland lows." - Same as *Tanaka et al., 2014* [eHh].	Volcanic, eolian, fluvial/lacustrine materials.
Vms	Valles Marineris skirting	Bright plains, low THEMIS nighttime temperature. Topographically smooth, very lightly cratered, contains small wrinkle ridges.	Plains unit along the rim of Valles Marineris.

Table 3: Description of geomorphic map units in deposit region.

5 Discussion and Interpretation

5.1 Deposit Region

While some units in the deposit region exactly match the description and interpretation of units in Tanaka et al., 2014 (e.g., mNh and eHt), others do not (see Table 1). For example, a departure from the global map is the unit we designate lNh, which merges relevant parts of the descriptions and interpretations from the global [lNh] and [eHt]. This is likely a result of mapping at a finer scale within a "transition zone". Higher resolution images show mounds and mesas within the wrinkle ridged plains, not separated. The unit we designate Cs is also not present within the global map, yet can be identified at both our map scale and at the global map scale. We assume from the slope of the Cs unit and the cross cutting of Hypanis Valles that Cs underlies the Hypanis deposit, and filled the southern Chryse region prior to Cd and lNh (Figure 10).

The Lederberg crater region has previously been interpreted by Brož and Hauber (2013). We agree with their interpretations that floor unit (Lf1) contains explosive and effusive volcanic features including breached cones (perhaps from hydrovolcanic eruptions), volcanos, and dark flows. We interpret the higher relief ridges, mounds, and dark valleys in the Lederberg rim unit (Lr) to be erupted material that later followed fractures and conduits from the Lederberg impact. The plains Lederberg floor unit (Lf2) closely resembles

Pf and other mantling plains in the region, thus we assume formation occurred by a similar mechanism.

Crater and channel units within the detailed deposit map follow descriptions and interpretations as presented in other works in greater detail including Goudge et al., 2015, Hynek et al., 2010, Fawdon et al., 2018, Knade et al., 2017, and Adler et al., 2019. One exception is the Crater pitted apron unit (Cpa) with a unique morphology that is only present where possibly mantling a Hypanis delta lobe (see Fawdon et al., 2018 figure 7a).

We interpret six units as volcanic in origin. Dark flows (Df) are interpreted as volcanic due to crater-retention, lower albedo, flow-like margins, widespread occurrence in topographic lows, as plains, or as a flat capping unit. Plateaus or mesas (Pl) we also interpret as possibly volcanic material due to similar morphologies as (Df) as the top material of some of these features. We interpret these isolated plateaus as highly eroded due to their shape and separation from one another, which suggests a high-standing continuous layer now broken apart.

The interpretation of regional volcanic activity extends more widely than in the mapped deposit region. Cone and mound shaped features are widespread in the Chryse Planitia, Acidalia Planitia, Arabia Terra, and Chryse outflow regions. Mounds and cones with varying morphometric properties in the broader region have been interpreted as either igneous eruption features or sedimentary eruption (e.g. mud volcano) features (Harrison et al., 2012; Meresse et al., 2008; Hauber et al., 2015; Brož et al., 2015; Farrand et al., 2005; Komatsu et al., 2016; Tanaka et al., 1999; Okubo et al., 2009; Oehler and Allen, 2010; Dapremont and Wray, 2021). While we cannot be certain without further data or analysis, we favor a sedimentary volcanic interpretation for these features.

Cones and mounds appear to be the youngest geologic units in the region. Three observations support this interpretation that the formation of cones and mounds is the most recent observable local activity, post-dating the Hypanis light toned layered fan deposit. 1) These cones and mounds superpose or overlap impact craters in unit lNh (Figure 8). 2) They appear to emerge through the Hypanis deposit (unit Cd or Fd) without diverting paleoflow lineations. 3) They appear to have a "fresh" surface morphology in HiRISE images in both types of mounds observed. These two morphologies are: small pitted texture which appears crisp not degraded or filled; and a dark rough texture appearing crisp not degraded. Cones

and mounds appear younger than the late Noachian due to stratigraphic relations with unit lNh and wrinkle ridges.

A recent publication (McNeil et al., 2021) mapped many of the same "isolated landform" features we have also identified and at a much wider scale in three zones around Chryse Planitia. McNeil et al. (2021) classified landforms into four classes based on morphology and came to two conclusions which are not supported by our work further examining mounds and cones in the Hypanis deposit region (their Zone 3). One conclusion was that the mounds were layered. This is generally not true in the Hypanis region from examining HiRISE and CTX images of most of these features. Another conclusion put forth in McNeil et al. (2021) was that an extensive contiguous layer (or layers) at least 500 m thick covered the circum-Chryse region and has been eroded down to create these isolated landforms. While this is possible for plateaus, which are irregularly shaped, have some layering, and likely extended beyond their current truncated extent (see Figure 5a), cones and mounds make up a majority of the mapped features and do not contain this layering. Furthermore, cones are round and have central craters. Their setting and morphology are clearly volcanic and thus the conclusion that these are eroded rounded remnants of a thick plateau unit is likely flawed. McNeil et al. (2021) suggests that mounds are embayed by the Chryse Planitia plains and are therefore Noachian in age, but we did not see evidence of this relationship.

Figure 8: A 600 m wide mound overlaps a crater in unit lNh, thus indicating the mound formed after lNh.

The broader area mapping of McNeil et al. is nonetheless very useful and timely, as there appears to be a connection between isolated landforms near Hypanis and those near the ExoMars Rosalind Franklin rover landing site in Oxia Planum. Thus, our mapping and this prior work suggests a wider depositional and erosional history than at each individual site. This warrants future investigation as similarities between the ExoMars and our mapped region are striking (Früh et al., 2021).

The coexistence of faults, wrinkle ridges, buried crater rims, and volcanic features in the deposit map region suggests that the erupted materials might have used existing faults and fractures as conduits to the surface. Some cones and mounds appear to have experienced further faulting or some degree of internal collapse after formation. For the faulted mounds that formed along wrinkle ridges, this may indicate reactivation of wrinkle ridge tectonism or co-formation around 3.2 Ga. In most cases, however, cones and mounds along wrinkle ridges are not faulted, implying formation after wrinkle ridge activity. Cases like the one shown in Figure 8 superimpose craters in the plains material, demonstrating that the plains do not embay these mounds, but that the mounds erupt through the plains.

We hypothesize that cones and mounds in the deposit region may have been formed by mud volcanism or sedimentary diapirism. This would be consistent with the interpretations of other nearby studies (Farrand et al., 2005; Komatsu et al., 2016; Tanaka et al., 1999; Okubo et al., 2009; Oehler and Allen, 2010) and is consistent with expectation for a tectonically compressed sedimentary basin (Skinner and Mazzini, 2009). The Chryse basin experienced repeated burial of water-rich sediments by fluvial activity and regional plains style and explosive volcanism, thus several reasonable mechanisms for eruption of buried material could be proposed. More work is needed to properly investigate a sedimentary eruption formation mechanism of these cone and mound features, including remote analysis, numeric modeling, and lab experiments.

5.2 Catchment Region

The materials in the Hypanis Valles catchment are diverse in age and origin because the Hypanis Valles and Nanedi Valles systems are extensive. The mapped Noachian units contain reworked impact, volcanic, and fluvial materials as interpreted by many works including the Tanaka et al., 2014 map with which our work generally agrees.
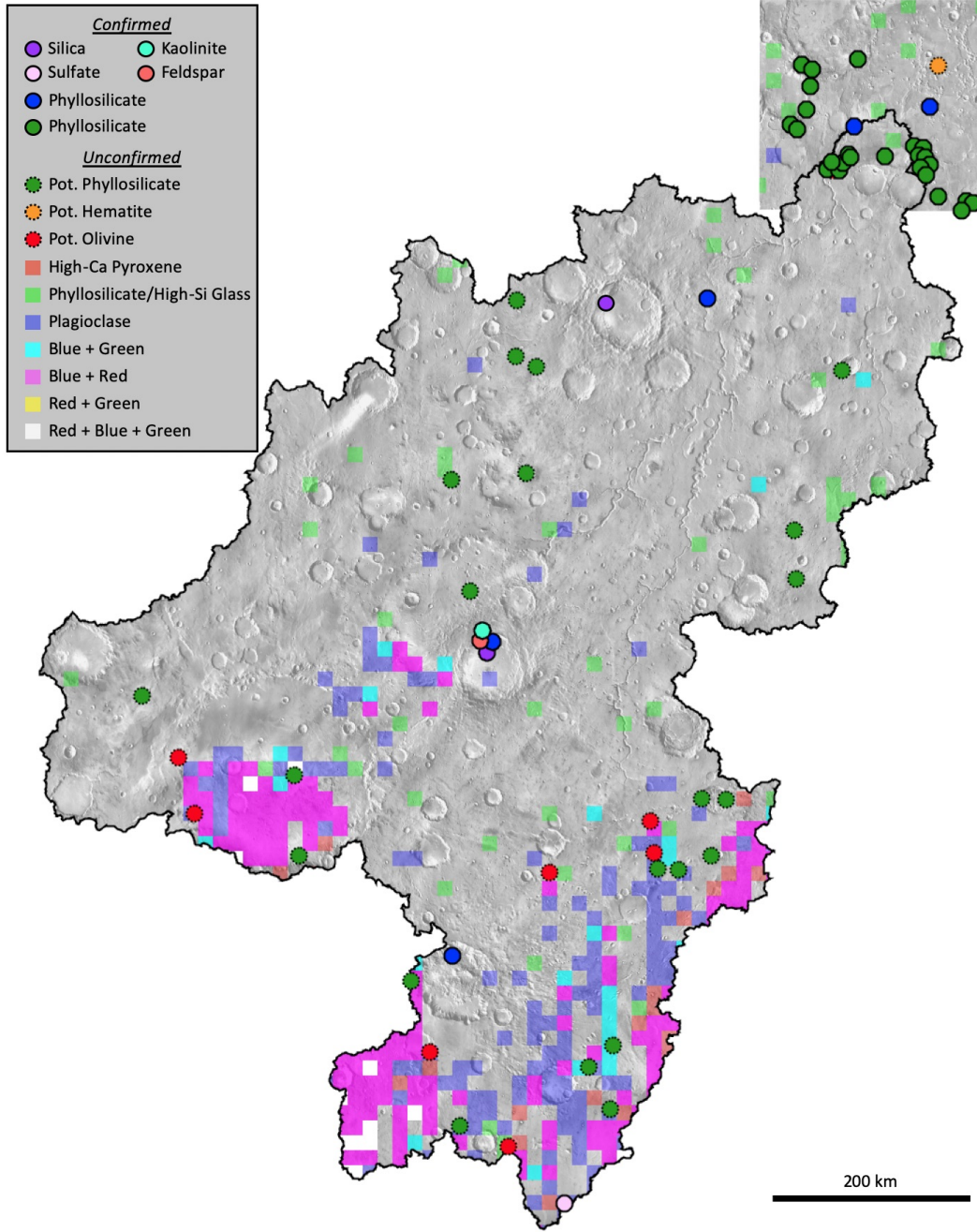
Figure 9: Minerals identified in the Hypanis catchment and deposit region. Confirmed mineral locations are derived from a variety of publications. Unconfirmed are presented in this work. Confirmed: hydrated silica, kaolinite, and feldspar [Wray et al., 2013; Carter and Poulet, 2013; Pan et al., 2021]; hydrated sulfate, phyllosilicate [Carter et al., 2014, Ehlmann and Edwards, 2014 and references therein]; phyllosilicate (green) [Adler et al., 2019]. Unconfirmed: phyllosilicate [CRISM MSP, D2300 parameter > 0.05]; hematite [TES Hematite Abundance > 0.10, Bandfield, 2002]; olivine [TES Olivine Abundance > 0.10, Koeppen and Hamilton, 2008]; high-Ca pyroxene [TES HCP Abundance > 0.10, Bandfield, 2002]; phyllosilicate/hi-Si glass [TES High-Si Glass Abundance > 0.10, Bandfield, 2002]; plagioclase [TES Plagioclase Abundance > 0.10, Bandfield, 2002]. Where multiple TES mineral abundance maps were above the 0.10 detection threshold described in Bandfield, 2002 for a given pixel, the color was the marked according to the legend.

Because the composition of the Hypanis deposit is unclear (due to dusty spectral observations), we broadly searched for compositional clues within the catchment and deposit region. Unfortunately, most of the catchment appears to have significant dust cover, and the largest relatively dust-free areas today occur in the southern distal catchment, a region of surfaces suspected to be younger than the age of Hypanis sedimentation. To search for the best time to examine older dust free surfaces that were more likely to have contributed to Hypanis, we analyzed MARCI albedo videos for Mars years 28-33 (Wellington and Bell., 2020). The video for the Lunae Palus quad did not show a darkening pattern to constrain our search. Thus, we caution that the mineralogy identified in Figure 9 is biased toward locations where CRISM high resolution images exist, and locations that are less dusty in the distal catchment.

Despite these limitations, several components have been identified including basaltic endmembers and widespread alteration minerals. Scattered throughout the proximal and middle catchment areas, phyllosilicate and pyroxene observations have been reported by multiple sources (Figure 9). This has been shown to be ubiquitous for Noachian-aged highland terrain, and is thus expected (Ehlmann and Edwards, 2014). No clear clumping or spatially consistent patterns are identified at our scale in the proximal and mid-catchment. A unique locality mid-catchment was found to contain Felsic rocks near hydrated silica and kaolinite (Wray et al., 2013; Carter and Poulet, 2013; Pan et al., 2021). In the distal catchment a basaltic component was inferred from the combination of pyroxene and plagioclase in quantities well above the detection threshold (pink squares in Figure 9). These surfaces were mapped as Ri, Sp, Vms, and possibly Rl (Figure 7). In lower albedo locations, this pyroxene and plagioclase signature appears to correspond to exposures of eNh in the distal catchment. This would suggest, as expected, a basaltic component to the early Noachian highlands materials, through which Hypanis Valles formed. The presence of olivine as well in the distal catchment supports the volcanic origin of a significant component of these materials.

Several types of crater morphologies in the catchment and deposit region were observed. We noted slurry ejecta and floor filled craters with medium to large diameters, suggesting agreement with a late Noachian to early Hesperian age (Tanaka et al., 2014). These craters with slurry ejecta and and/or with central pits have morphologies indicative of volatiles either on the surface or at depth. Their stratigraphic relations imply that ice depth decreased with time as noted by Reiss et al. (2006). Pedestal craters identified
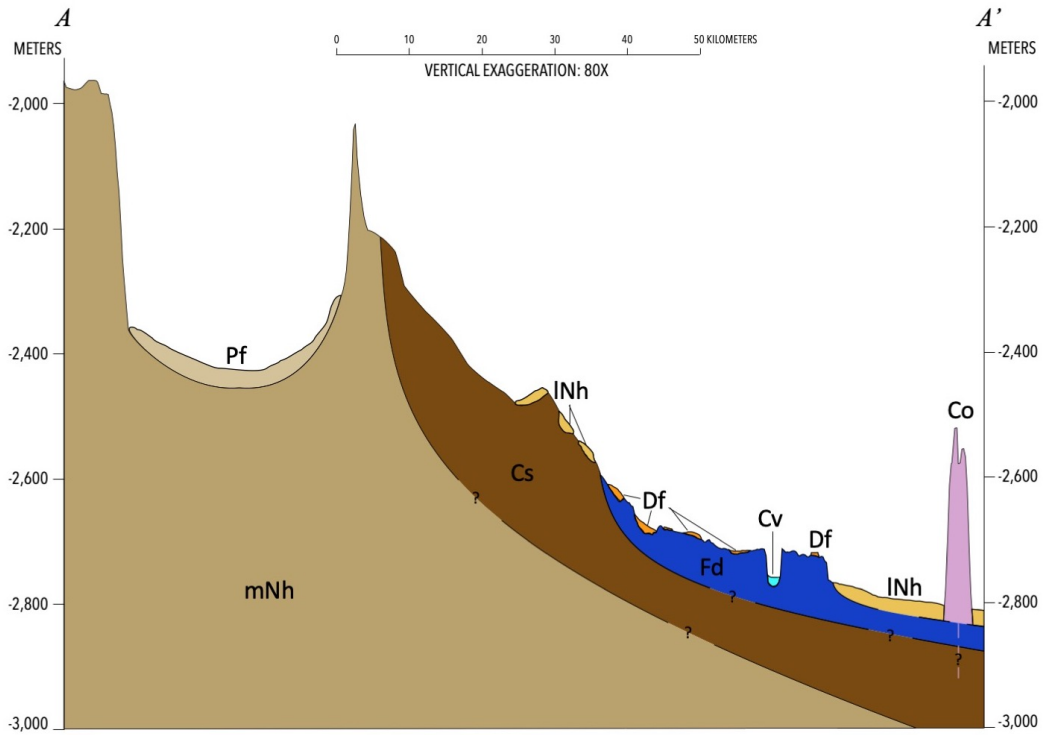
Figure 10: Cross section of Hypanis deposit region showing interpreted and unknown stratigraphy under traverse A-A' marked in Figure 4.

438 were much smaller in diameter, and the most recent impacts (Cde) and (Cy) were likely

439 too small to penetrate to a subsurface ice layer (if it remained) and produce ice-influenced

440 morphologies.

5.3 No Evidence of a Land Dam Ponding a Southern Chryse Lake

442 The current topography of the Chryse basin is unconfined to the north at the elevations

443 of the Hypanis deposit. Thus, if 1) Hypanis was truly formed subaqueously and if 2)

444 the regional topography was not much different than today, then there must have been a

445 northern ocean. Our mapping partly addressed the latter condition, and found no evidence

446 of an ancient land dam that could have ponded water locally in the late Noachian. Others

447 have suggested the rounded buttes and mesas are a sign of a previously larger unit to the

448 north, but timing for formation of these features is post-Hypanis, and their eruptive origins

449 do not support this claim. Further work could examine the role of ice or glaciers in the

450 formation of Hypanis and determine if an ice dam would be plausible.

6 Conclusions

We created geomorphic maps of the Hypanis Valles watershed and of the Hypanis deposit region. We defined map units both quantitatively and qualitatively from orbital images, and datasets. Units were designated according to their morphology, albedo, thermal inertia, and spectral signature. Hypanis Valles carved through several unique Noachian units older than most terrain surrounding the Chryse basin. Evidence of recent and ancient volcanic activity is present in the catchment and basin. Hypanis Valles was fluvially active throughout the Noachian and formed the terminal deposit in the late Noachian. As proposed in prior works, Hypanis may have formed subaqueously as a delta, and may record a water level drop of about 500 m as a shoreline retreated to the northeast. We identified kilometer-sized cones and mounds which appear to have erupted onto the surface. Characteristics of these features more strongly resemble outgassing, sedimentary diapirism, and mud volcanism than igneous volcanism. Future work should determine if Mars erupted sediments and volatiles in this region, and by what mechanism. Further study of the deposit map region may be relevant for understanding the current extent of buried reservoirs of volatiles in sedimentary basins on Mars, and study of the Hypanis system may further contribute to our understanding of the total inventory of water on Mars in the Noachian.

7 Supplementary Material

GIS-ready .zip file of mapped shapes.

References

Adler, J. B., Bell III, J. F., Fawdon, P., Davis, J., Warner, N. H., Sefton-Nash, E., & Harrison, T. N. (2019). Hypotheses for the origin of the Hypanis fan-shaped deposit at the edge of the Chryse escarpment, Mars: Is it a delta? *Icarus*, *319*, 885–908. Retrieved from https://doi.org/10.1016/j.icarus.2018.05.021

Arvidson, R. E., Bonitz, R. G., Robinson, M. L., Carsten, J. L., Volpe, R. A., Trebi-Ollennu, A., . . . Others (2009). Results from the Mars Phoenix lander robotic arm experiment. *Journal of Geophysical Research: Planets*, *114*(E1).

Baker, V. R., Strom, R. G., Gulick, V. C., Kargel, J. S., Komatsu, G., & Kale, V. S. (1991). Ancient oceans, ice sheets and the hydrological cycle on Mars. *Nature*, *352*(6336), 589–594. doi: 10.1038/352589a0

Bandfield, J. L. (2002). Global mineral distributions on Mars. *Journal of Geophysical Research: Planets*, *107*(E6), 1–9.

Brož, P., Čadek, O., Hauber, E., & Rossi, A. P. (2015). Scoria cones on Mars: Detailed investigation of morphometry based on high-resolution digital elevation models. *Journal of Geophysical Research: Planets*, *120*(9), 1512–1527.

Brož, P., & Hauber, E. (2013). Hydrovolcanic tuff rings and cones as indicators for phreatomagmatic explosive eruptions on Mars. *Journal of Geophysical Research: Planets*, *118*(8), 1656–1675. doi: 10.1002/jgre.20120

Cabrol, N. A., & Grin, E. A. (1999). Distribution, Classification, and Ages of Martian Impact Crater Lakes. *Icarus*, *142*(1), 160–172. doi: 10.1006/ICAR.1999.6191

Cabrol, N. A., & Grin, E. A. (2001). The Evolution of Lacustrine Environments on Mars: Is Mars Only Hydrologically Dormant? *Icarus*, *149*(2), 291–328. doi: 10.1006/ICAR.2000.6530

Carr, M. H. (1996). *Water on Mars.* Oxford University Press.

Carr, M. H. (2000). Martian oceans, valleys and climate. *Astronomy and Geophysics*, *41*(3), 3.20–3.26. doi: 10.1046/j.1468-4004.2000.00320.x

Carr, M. H., & Head, J. W. (2009). Geologic history of Mars. *Earth and Planetary Science Letters*, *294*, 185–203. doi: 10.1016/j.epsl.2009.06.042

Carter, J., Loizeau, D., Mangold, N., Poulet, F., & Bibring, J.-P. (2015). Widespread surface weathering on early Mars: A case for a warmer and wetter climate. *Icarus*, *248*, 373–382.

Carter, J., & Poulet, F. (2013). Ancient plutonic processes on Mars inferred from the

detection of possible anorthositic terrains. *Nature Geoscience*, *6*(12), 1008–1012.

Christensen, P. R., Engle, E., Anwar, S., Dickenshied, S., Noss, D., Gorelick, N., & Weiss-Malik, M. (2009). JMARS - A Planetary GIS. *American Geophysical Union, Fall Meeting 2009, abstract id.IN22A-06*.

Citron, R. I., Manga, M., & Hemingway, D. J. (2018). Timing of oceans on Mars from shoreline deformation. *Nature*, *555*(7698), 643.

Clifford, S. M., & Parker, T. J. (1999). Hydraulic and Thermal Arguments Regarding the Existence and Fate of a Primordial Martian Ocean. *30th Annual Lunar and Planetary Science Conference, March 15-29, 1999, Houston, TX, abstract no. 1619*, *30*.

Clifford, S. M., & Parker, T. J. (2001). The Evolution of the Martian Hydrosphere: Implications for the Fate of a Primordial Ocean and the Current State of the Northern Plains. *Icarus*, *154*, 40–79. doi: 10.1006

Dapremont, A. M., & Wray, J. J. (2021). Igneous or Mud Volcanism on Mars? The Case Study of Hephaestus Fossae. *Journal of Geophysical Research: Planets*, *126*(2), e2020JE006390.

Di Achille, G., & Hynek, B. M. (2010). Ancient ocean on Mars supported by global distribution of deltas and valleys. *Nature Geoscience*, *3*(7), 459–463. doi: 10.1038/ngeo891

Dickson, J. L., Kerber, L. A., Fassett, C. I., & Ehlmann, B. L. (2018). A global, blended CTX mosaic of Mars with vectorized seam mapping: A new mosaicking pipeline using principles of non-destructive image editing. In *Lunar and planetary science conference* (Vol. 49, pp. 1–2).

Ehlmann, B. L., & Edwards, C. S. (2014). Mineralogy of the Martian Surface. *Annual Review of Earth and Planetary Sciences*, *42*(1), 291–315. doi: 10.1146/annurev-earth-060313-055024

Esri, A. D. (2011). Release 10. *Documentation Manual. Redlands, CA, Environmental Systems Research Institute*.

Farrand, W. H., Gaddis, L. R., & Keszthelyi, L. (2005). Pitted cones and domes on Mars: Observations in Acidalia Planitia and Cydonia Mensae using MOC, THEMIS, and TES data. *Journal of Geophysical Research: Planets*, *110*(E5).

Fassett, C. I., & Head, J. W. (2008). The timing of martian valley network activity: Constraints from buffered crater counting. *Icarus*, *195*(1), 61–89. doi: 10.1016/J.ICARUS.2007.12.009

544 Fassett, C. I., & Head III, J. W. (2005). Fluvial sedimentary deposits on Mars: Ancient
545   deltas in a crater lake in the Nili Fossae region. *Geophysical Research Letters*, *32*(14).

546 Fassett, C. I., & Head III, J. W. (2008). Valley network-fed, open-basin lakes on Mars:
547   Distribution and implications for Noachian surface and subsurface hydrology. *Icarus*,
548   *198*(1), 37–56.

549 Fawdon, P., Gupta, S., Davis, J. M., Warner, N. H., Adler, J. B., Balme, M. R., . . . Sefton-
550   Nash, E. (2018). The Hypanis Valles delta: The last highstand of a sea on early Mars?
551   *Earth and Planetary Science Letters*, *500*, 225–241. doi: 10.1016/J.EPSL.2018.07.040

552 Fergason, R. L., Christensen, P. R., & Kieffer, H. H. (2006). High-resolution thermal inertia
553   derived from the Thermal Emission Imaging System (THEMIS): Thermal model and
554   applications. *J. Geophys. Res*, *111*. doi: 10.1029/2006JE002735

555 Früh, T., Hauber, E., Adeli, S., Tirsch, D., & Nass, A. (2021). Northern Xanthe Terra:
556   A Reference Site to Test Hypotheses Related to the Oxia Planum Landing Site for
557   ExoMars 2022. In *Lunar and planetary science conference* (p. 1977).

558 Goldspiel, J. M., & Squyres, S. W. (1991). Ancient aqueous sedimentation on Mars. *Icarus*,
559   *89*(2), 392–410.

560 Goudge, T. A., Mustard, J. F., Head, J. W., Fassett, C. I., & Wiseman, S. M. (2015).
561   Assessing the mineralogy of the watershed and fan deposits of the Jezero crater pale-
562   olake system, Mars. *Journal of Geophysical Research: Planets*, *120*(4), 775–808. doi:
563   10.1002/2014JE004782

564 Harrison, T. N. (2012). Evidence for Volcanism in and Near the Chaotic Terrains East of
565   Valles Marineris, Mars. *43rd Lunar and Planetary Science Conference, held March*
566   *19-23, 2012 at The Woodlands, Texas. LPI Contribution No. 1659, id.1057*, *43*.

567 Hauber, E., Gwinner, K., Kleinhans, M., Reiss, D., Di Achille, G., Ori, G.-G., . . . Neukum,
568   G. (2009). Sedimentary deposits in Xanthe Terra: Implications for the ancient climate
569   on Mars. *Planetary and Space Science*, *57*(8-9), 944–957. doi: 10.1016/J.PSS.2008.06
570   .009

571 Head, J. W., Kreslavsky, M., Hiesinger, H., Ivanov, M., Pratt, S., Seibert, N., . . . Zuber,
572   M. T. (1998). Oceans in the past history of Mars: Tests for their presence using
573   Mars Orbiter Laser Altimeter (MOLA) data. *Geophysical Research Letters*, *25*(24),
574   4401–4404. doi: 10.1029/1998GL900116

575 Howard, A. D., Moore, J. M., & Irwin III, R. P. (2005). An intense terminal epoch of
576   widespread fluvial activity on early Mars: 1. Valley network incision and associated

deposits. *Journal of Geophysical Research: Planets*, *110*(E12).

Hynek, B. M., Beach, M., & Hoke, M. R. T. (2010). Updated global map of Martian valley networks and implications for climate and hydrologic processes. *Journal of Geophysical Research: Planets*, *115*(E9).

Irwin, R. P., Howard, A. D., Craddock, R. A., & Moore, J. M. (2005). An intense terminal epoch of widespread fluvial activity on early Mars: 2. Increased runoff and paleolake development. *Journal of Geophysical Research: Planets*, *110*(E12).

Irwin III, R. P., Craddock, R. A., & Howard, A. D. (2005). Interior channels in Martian valley networks: Discharge and runoff production. *Geology*, *33*(6), 489–492.

Kleinhans, M. G., van de Kasteele, H. E., & Hauber, E. (2010). Palaeoflow reconstruction from fan delta morphology on Mars. *Earth and Planetary Science Letters*, *294*(3-4), 378–392. doi: 10.1016/J.EPSL.2009.11.025

Knade, J., Hauber, E., Platz, T., Le Deit, L., & Kinch, K. (2017). Detailed geological mapping of the fluvial deposits in Magong crater, Xanthe Terra, Mars.

Koeppen, W. C., & Hamilton, V. E. (2008). Global distribution, composition, and abundance of olivine on the surface of Mars from thermal infrared data. *Journal of Geophysical Research: Planets*, *113*(E5).

Komatsu, G., Okubo, C. H., Wray, J. J., Ojha, L., Cardinale, M., Murana, A., . . . Gallagher, R. (2016). Small edifice features in Chryse Planitia, Mars: assessment of a mud volcano hypothesis. *Icarus*, *268*, 56–75.

Luo, W., Cang, X., & Howard, A. D. (2017). New Martian valley network volume estimate consistent with ancient ocean and warm and wet climate. *Nature communications*, *8*, 15766.

McNeil, J. D., Fawdon, P., Balme, M. R., & Coe, A. L. (2021). Morphology, Morphometry and Distribution of Isolated Landforms in Southern Chryse Planitia, Mars. *Journal of Geophysical Research: Planets*, *126*(5).

Meresse, S., Costard, F., Mangold, N., Masson, P., Neukum, G., & Others. (2008). Formation and evolution of the chaotic terrains by subsidence and magmatism: Hydraotes Chaos, Mars. *Icarus*, *194*(2), 487–500.

Oehler, D. Z., & Allen, C. C. (2010). Evidence for pervasive mud volcanism in Acidalia Planitia, Mars. *Icarus*, *208*(2), 636–657.

Oehler, D. Z., & Allen, C. C. (2012). Giant polygons and mounds in the lowlands of Mars: signatures of an ancient ocean? *Astrobiology*, *12*(6), 601–615.

Okubo, C. H. (2016). Morphologic evidence of subsurface sediment mobilization and mud volcanism in Candor and Coprates Chasmata, Valles Marineris, Mars. *Icarus*, *269*, 23–37.

Pan, L., Carter, J., Quantin-Nataf, C., Pineau, M., Chauviré, B., Mangold, N., . . . Chevrier, V. (2021). Voluminous silica precipitated from martian waters during late-stage aqueous alteration. *The Planetary Science Journal*, *2*(2), 65.

Pan, L., Quantin-Nataf, C., Breton, S., & Michaut, C. (2019). The impact origin and evolution of Chryse Planitia on Mars revealed by buried craters. *Nature communications*, *10*(1), 1–8.

Parker, T. J. (1994). Martian Paleolakes and Oceans. *Thesis (PH.D.)–University of Southern California, 1994.Source: Dissertation Abstracts International, Volume: 56-09, Section: B, page: 4789.*.

Perron, J. T., Mitrovica, J. X., Manga, M., Matsuyama, I., & Richards, M. A. (2007). Evidence for an ancient martian ocean in the topography of deformed shorelines. *Nature*, *447*(7146), 840–843.

Pieri, D. C. (1980). Martian valleys: Morphology, distribution, age, and origin. *Science*, *210*(4472), 895–897.

Reiss, D., Gasselt, S., Hauber, E., Michael, G., Jaumann, R., & Neukum, G. (2006). Ages of rampart craters in equatorial regions on Mars: Implications for the past and present distribution of ground ice. *Meteoritics & Planetary Science*, *41*(10), 1437–1452. doi: 10.1111/j.1945-5100.2006.tb00428.x

Rodriguez, J. A. P., Fairén, A. G., Tanaka, K. L., Zarroca, M., Linares, R., Platz, T., . . . Others (2016). Tsunami waves extensively resurfaced the shorelines of an early Martian ocean. *Scientific reports*, *6*, 25106.

Rotto, S., & Tanaka, K. L. (1995). *Geologic, Geomorphologic Map of the Chryse Planitia Region of Mars.* USGS.

Scheller, E. L., Ehlmann, B. L., Hu, R., Adams, D. J., & Yung, Y. L. (2021). Long-term drying of Mars by sequestration of ocean-scale volumes of water in the crust. *Science*, *372*(6537), 56–62.

Scott, D., & Tanaka, K. (1986). *Geologic map of the western equatorial region of Mars* (Tech. Rep.). Retrieved from `https://pubs.er.usgs.gov/publication/i1802A` doi: 10.3133/i1802A

Scott, D. H., & Carr, M. H. (1978). *Geologic map of Mars* (Tech. Rep.). doi: 10.3133/i1083

Sholes, S. F., Dickeson, Z. I., Montgomery, D. R., & Catling, D. C. (2021). Where are Mars' Hypothesized Ocean Shorelines? Large Lateral and Topographic Offsets Between Different Versions of Paleoshoreline Maps. *Journal of Geophysical Research: Planets*, *126*(5), e2020JE006486.

Sholes, S. F., Montgomery, D. R., & Catling, D. C. (2019). Quantitative High-Resolution Reexamination of a Hypothesized Ocean Shoreline in Cydonia Mensae on Mars. *Journal of Geophysical Research: Planets*, *124*(2), 316–336.

Skinner Jr, J. A., & Mazzini, A. (2009). Martian mud volcanism: Terrestrial analogs and implications for formational scenarios. *Marine and Petroleum Geology*, *26*(9), 1866–1878.

Skinner Jr, J. A., & Tanaka, K. L. (2007). Evidence for and implications of sedimentary diapirism and mud volcanism in the southern Utopia highland–lowland boundary plain, Mars. *Icarus*, *186*(1), 41–59.

Smith, P. H., Tamppari, L. K., Arvidson, R. E., Bass, D., Blaney, D., Boynton, W. V., . . . Others (2009). H2O at the Phoenix landing site. *Science*, *325*(5936), 58–61.

Tanaka, K. L. (1997). Sedimentary history and mass flow structures of Chryse and Acidalia Planitiae, Mars. *Journal of Geophysical Research: Planets*, *102*(E2), 4131–4149. doi: 10.1029/96JE02862

Tanaka, K. L. (1999). Debris-flow origin for the Simud/Tiu deposit on Mars. *Journal of Geophysical Research: Planets*, *104*(E4), 8637–8652.

Tanaka, K. L., Skinner Jr, J. A., Dohm, J. M., Irwin III, R. P., Kolb, E. J., Fortezzo, C. M., . . . Hare, T. M. (2014). Geologic map of Mars. *U.S. Geological Survey Scientific Investigations Map 3292, scale 1:20,000,000, pamphlet 43 p.*. doi: 10.3133/sim3292

Villanueva, G. L., Mumma, M. J., Novak, R. E., Käufl, H. U., Hartogh, P., Encrenaz, T., . . . Smith, M. D. (2015). Strong water isotopic anomalies in the martian atmosphere: Probing current and ancient reservoirs. *Science*, *348*(6231), 218–221.

Viviano-Beck, C. E., Seelos, F. P., Murchie, S. L., Kahn, E. G., Seelos, K. D., Taylor, H. W., . . . Morgan, M. F. (2014). Revised CRISM spectral parameters and summary products based on the currently detected mineral diversity on Mars. *Journal of Geophysical Research: Planets*, *119*(6), 1403–1431. doi: 10.1002/2014JE004627

Wellington, D. F., & Bell III, J. F. (2020). Patterns of surface albedo changes from Mars Reconnaissance Orbiter Mars Color Imager (MARCI) observations. *Icarus*, *349*, 113766.

Wray, J. J., Hansen, S. T., Dufek, J., Swayze, G. A., Murchie, S. L., Seelos, F. P., . . .

676   Ghiorso, M. S. (2013). Prolonged magmatic activity on Mars inferred from the detec-

677   tion of felsic rocks. *Nature Geoscience*, *6*(12), 1013–1017.